32ND INTERNATIONAL COSMIC RAY CONFERENCE, BEIJING 2011

Study of South Pole ice transparency with IceCube flashers

THE ICECUBE COLLABORATION[1]
[1]*See special section in these proceedings*

Abstract: The IceCube observatory, 1 km^3 in size, is now complete with 86 strings deployed in the antarctic ice. IceCube detects the Cherenkov radiation emitted by charged particles passing through or created in the ice. To realize the full potential of the detector the properties of light propagation in the ice in and around the detector must thus be known to the best achievable accuracy. This report presents a new method of fitting the ice model to a data set of in-situ light source events collected with IceCube. The resulting set of derived ice parameters is presented and a comparison of IceCube data with simulation based on the new model is shown.

Corresponding author: Dmitry Chirkin (*dima@icecube.wisc.edu*)
IceCube Reseach Center, University of Wisconsin, Madison, WI 50703, U.S.A.

Keywords: IceCube, ice properties, ice transparency, scattering, absorption, photon propagation

1 Introduction

The properties of photon propagation in a transparent medium can be described in terms of the average distance between successive scatters and the average distance to absorption (local scattering and absorption lengths), as well as the angular distribution of the new direction of a photon relative to old at a given scattering point. These details are used in both the simulation and reconstruction of IceCube data, thus they must be known to the best possible accuracy. This work presents a new, *direct fit* approach to determine these ice properties, which is different from the method described in [4]. A global fit is performed to a set of data with in-situ light sources (see Figure 1) covering all depths of the detector, resulting in a single set of scattering and absorption parameters of ice, which describes these data best. Figure 2 shows examples of experimental data used for this analysis.

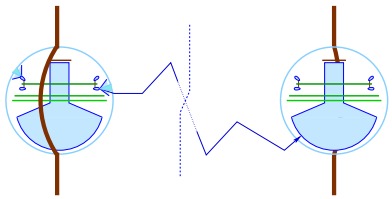

Figure 1: Simplified schematics of the experimental setup: the flashing sensor on the left emits photons, which propagate through ice and are detected by a receiving sensor on the right.

2 Flasher dataset

In 2008, IceCube consisted of 40 strings as shown in Figure 3, each equipped with 60 equally spaced optical sensors, or digital optical modules (DOMs). Each of the DOMs consists of a 10” diameter photomultiplier tube (PMT) [2] and several electronics boards enclosed in a glass container [3]. One of the boards is the ”flasher board”, which has 6 horizontal and 6 tilted LEDs, each capable of emitting $\sim 7.5 \cdot 10^9$ photons at $\sim 405 \pm 5$ nm in a 62 ns-wide pulse.

The PMT output signal is digitized into ”waveforms” using the faster, ATWD, and slower, fADC, sampling chips [1]. The ATWD is configured to collect 128 samples with 3.3 ns sampling rate, and the fADC records 256 samples with 25 ns sampling rate. The DOMs transmit time-stamped digitized PMT signal waveforms to computers at the surface.

In a series of several special-purpose runs, IceCube took data with each of 60 DOMs on string 63 flashing in a sequence. For each of the flashing DOMs at least 250 flasher events were collected and used in this analysis. All 6 horizontal LEDs were used simultaneously at maximum brightness and pulse width settings, creating a pattern of light around string 63 that is approximately azimuthally symmetric.

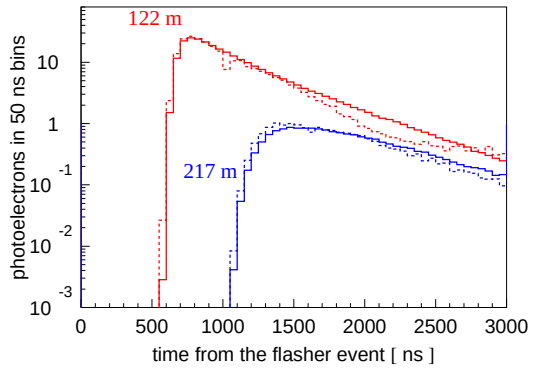

Figure 2: Example photon arrival time distributions at a sensor on one of the nearest strings (122 m away), and on one of the next-to-nearest strings (217 m away). Dashed lines show data and solid lines show simulation based on the model of this work (with best fit parameters). The goal of this work is to find the best-fit ice parameters, which describe these distributions as observed in data simultaneously for all pairs of emitters and receivers.

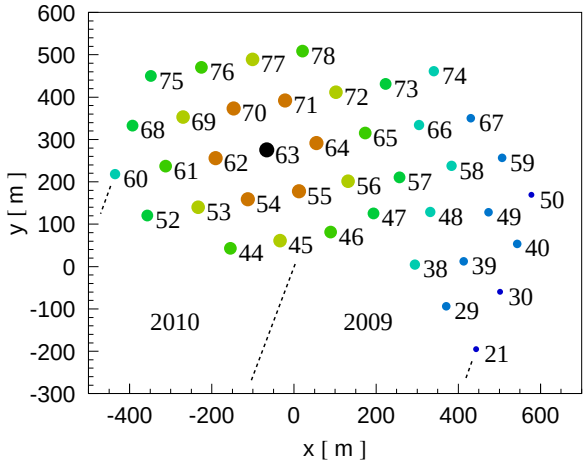

Figure 3: IceCube 40-string configuration as operated in 2008. String 63 (of DOMs that were used as flashers) is shown in black. IceCube parts installed in the following years (2009, 2010 as shown in the figure) lie in regions indicated approximately with dashed lines.

The pulses corresponding to the arriving photons were extracted from the digitized waveforms and binned in 25 ns bins, from 0 to 5000 ns from the start of the flasher pulse (extracted from the special-purpose ATWD channel of the flashing DOM). To reduce the contribution from saturated DOMs (most of which were on string 63 near the flashing DOM) [2] the photon data collected on string 63 was not used in the fit.

3 Ice parametrization

The ice is described by a table of parameters $b_e(405)$, $a(405)$, related to scattering and absorption at a wavelength of 405 nm at different depths. The width of the vertical ice layers (10 m) was chosen to be as small as possible while maintaining at least one receiving DOM in each layer. Coincidentally it is the same as the value chosen in [4].

The geometrical scattering coefficient b determines the average distance between successive scatters (as $1/b$). It is often more convenient to quote the effective scattering coefficient, $b_e = b \cdot (1 - \langle \cos\theta \rangle)$, where θ is the deflection angle at each scatter, $\langle\rangle$ denote the expectation value. The absorption coefficient a determines the average distance traveled by photon before it is absorbed (as $1/a$).

4 Simulation

The detector response to flashing each of the 60 DOMs on string 63 needs to be simulated very quickly, so that simulations based on many different sets of coefficients $b_e(405)$ and $a(405)$ could be compared to the data.

A program called PPC (photon propagation code [7]), was written for this purpose. It propagates photons through ice described by a selected set of parameters $b_e(405)$ and $a(405)$ until they hit a DOM or get absorbed. No special weighting scheme was employed, except that the DOMs were scaled up in size (a factor 5 to 16, depending on the required timing precision), and the number of emitted photons was scaled down by a corresponding factor ($5^2 - 16^2$).

The probability distribution $f(\theta)$ of the photon scattering angle θ is modeled by a linear combination of two functions commonly used to approximate scattering on impurities:

$$f(\theta) = (1 - f_{\mathsf{SL}}) \cdot \mathsf{HG} + f_{\mathsf{SL}} \cdot \mathsf{SL},$$

where HG is the Henyey-Greenstein function [4]:

$$p(\cos\theta) = \frac{1}{2} \frac{1 - g^2}{[1 + g^2 - 2g \cdot \cos\theta]^{3/2}}, \quad g = \langle \cos\theta \rangle,$$

and SL is the simplified Liu scattering function [8]:

$$p(\cos\theta) \sim (1 + \cos\theta)^{\alpha}, \quad \text{with} \quad \alpha = \frac{2g}{1 - g}.$$

f_{SL} determines the relative fraction of the two scattering functions and it determines the overall shape. Figure 4 compares these two functions with the prediction of the Mie theory with dust concentrations and radii distributions taken as described in [4]. The distributions of photon arrival time are substantially affected by the "shape" parameter f_{SL} (as shown in Figure 5). f_{SL} is also a global free parameter in the fitting procedure.

The value of $g = 0.9$ was used in this work (cf. $g = 0.8$ in [4]). Higher values (as high as ~ 0.94 [4, 6]) are predicted by the Mie scattering theory, however, these result

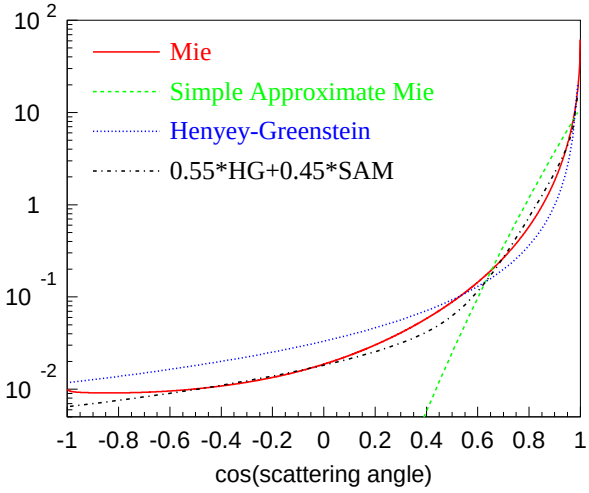

Figure 4: Comparison of the Mie scattering profiles calculated at several depths of the South Pole ice with the Henyey-Greenstein (HG) [4] and simplified Liu (SL) [8] scattering functions, all with the same $g = 0.943$.

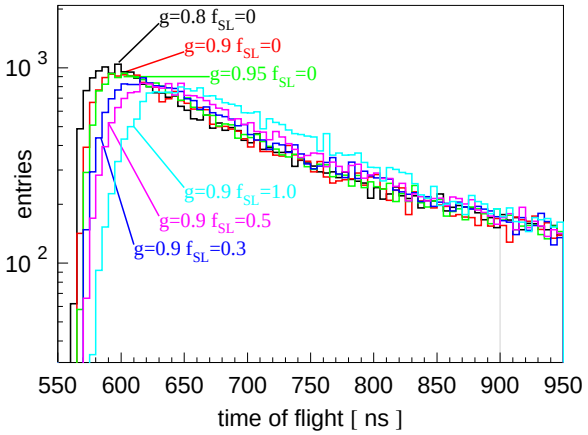

Figure 5: Photon arriving time distributions at a DOM 125 m away from the flasher, simulated for several values of $g = \langle \cos\theta \rangle$ and f_{SL}. The difference in peak position simulated with $g = 0.8$ and $g = 0.9$ is of the same order (~ 10 ns) as that between sets simulated with different values of the shape parameter f_{SL}.

in slower simulation, while yielding values of the effective scattering b_e and absorption a coefficients that change by less than 3% as determined in [4], which could also be concluded from Figure 5.

5 Fitting the flasher data

Data from all pairs of emitter-receiver DOMs (located in the same or different ice layers, altogether $\sim$ 38700 pairs) contributed to the fit of $\sim$ 200 ice parameters (scattering

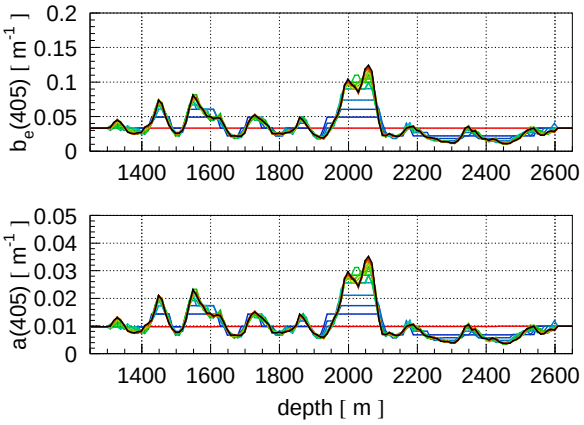

Figure 6: Values of $b_e(405)$ and $a(405)$ vs. depth for subsequent steps of the minimizer. The "converged" black curve shows fitted values after the last of the 20 steps of the minimizer.

and absorption in 10 m layers at detector depths of 1450 to 2450 m).

The photon counts $d(t_i)$ and $s(t_i)$ observed in time bins in n_d data and n_s simulated flasher events are compared to each other using a likelihood function

$$\mathcal{L} = \prod \frac{(\mu_s n_s)^s}{s!} e^{-\mu_s n_s} \cdot \frac{(\mu_d n_d)^d}{d!} e^{-\mu_d n_d} \cdot \frac{1}{\sqrt{2\pi}\sigma} \exp \frac{-(\log \mu_d - \log \mu_s)^2}{2\sigma^2} \cdot R.$$

The product is over all emitters and all time bins of receivers. $\mu_d(t_i)$ and $\mu_s(t_i)$ are the expected values of photon counts per event in data and simulation, and are determined by maximizing $\mathcal{L}$ with respect to these. The first two terms in the product are the Poisson probabilities, and the third term describes the systematic uncertainties inherent in the simulation. The last term R represents regularization constraints of the solution values with depth and with each other.

Starting with the homogeneous ice described with $b_e(405) = 0.042$ m^{-1} and $a(405) = 8.0$ km^{-1} (average of [4] at detector depths) the maximum of $\mathcal{L}$ is found in $\sim$ 20 steps. At each iteration step the values of $b_e(405)$ and $a(405)$ are varied in consecutive ice layers, one layer at a time. Five flashing DOMs closest to the layer, which properties are varied, are used to estimate the variation of the $\mathcal{L}$. Figure 6 shows ice properties after each of 20 steps of the minimizer. The general agreement of the model and data is good as shown in Figure 2.

6 Dust logger data

Several dust loggers [5] were used during the deployment of seven of the IceCube strings to result in a survey of the structure of ice dust layers with extreme detail (with the effective resolution of $\sim$ 2 millimeters). These were then matched up across the detector to result in a *tilt map* of the

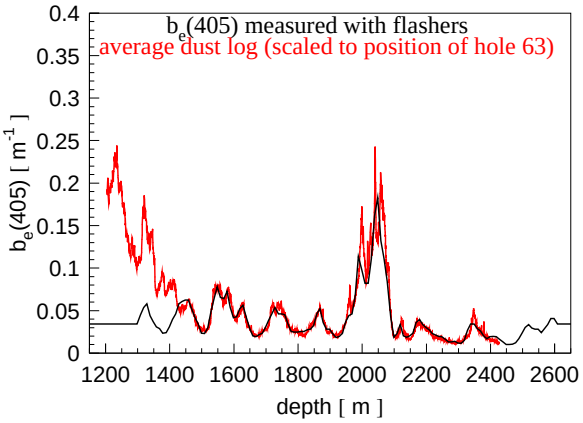

Figure 7: Comparison of the average dust log with the effective scattering coefficient $b_e(405)$ measured with the flasher data.

South Pole ice, as well as a high-detail *average dust log*, a record of a quantity proportional to the dust concentration vs. depth. Additionally, the EDML (East Dronning Maud Land, see [5]) ice core data was used to extend the dust record to below the lowest dust-logger-acquired point.

The correlation between the effective scattering coefficient measured with the IceCube flasher data and the average dust log (scaled to the location of string 63) is excellent, as shown in Figure 7. Within the depth range 1450 m - 2450 m instrumented with DOMs all major features match, have the right rise and falloff behavior, and are of the same magnitude. Some minor features are washed out in the flasher measurement.

Having established the correlation with the average dust log, the EDML-extended version of the log was used to build an initial approximation to the fitting algorithm described in the previous section. This resulted in a solution that is determined by the scaled values of the extended log (instead of by the somewhat arbitrary values of the initial homogeneous ice approximation) in the regions where the flasher fitting method has no resolving power, i.e., above and below the detector.

7 Results

The effective scattering and absorption parameters of ice measured in this work are shown in Figure 8 with the $\pm 10\%$ gray band corresponding to $\pm 1\sigma$ uncertainty at most depths. The uncertainty grows beyond the shown band at depths above and below the detector. The value of the scattering function parameter $f_{\mathrm{SL}} = 0.45$ was also determined.

Figure 8 also shows the AHA (Additionally Heterogeneous Absorption) model, which is based on the ice description of [4] extrapolated to cover the range of depths of IceCube and updated with a procedure enhancing the depth structure of the ice layers.

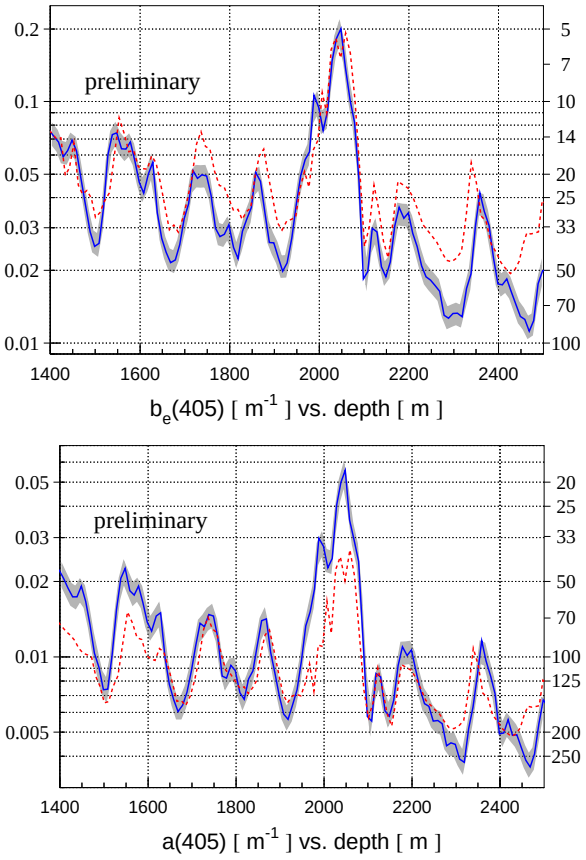

Figure 8: Values of $b_e(405)$ and $a(405)$ vs. depth for converged solution shown with solid lines. The updated model of [4] (AHA) is shown with dashed lines. The uncertainties of the AHA model at the AMANDA depths of 1730 ± 225 m are $\sim 5\%$ in b_e and $\sim 14\%$ in a. The scale and numbers to the right of each plot indicate the corresponding effective scattering $1/b_e$ and absorption $1/a$ lengths in meters.

References

[1] R. Abbasi et al., Nucl. Instrum. Methods A, 2009, **601**: 294-316.
[2] R. Abbasi et al., Nucl. Instrum. Methods A, 2010, **618**: 139-152.
[3] A. Achterberg et al., Astropart. Physics, 2006, **26**: 155.
[4] M. Ackermann et al., J. Geophys. Res., 2006, **111**: D13203.
[5] R. C. Bay et al., J. Geophys. Res., 2010, **115**: D14126.
[6] D. Chirkin., 2002, Mie scattering code and plots: http://icecube.wisc.edu/~dima/work/ICESCA.
[7] D. Chirkin., 2010, photon propagation code: http://icecube.wisc.edu/~dima/work/WISC/ppc.
[8] Pingyu Liu., Phys. Med. Biol., 1994, **39**: 1025.